Optical Engineering

SPIEDigitalLibrary.org/oe

# Monitoring the cementitious materials subjected to sulfate attack with optical fiber excitation Raman spectroscopy

Yanfei Yue
Yun Bai
P. A. Muhammed Basheer
John J. Boland
Jing Jing Wang

# Monitoring the cementitious materials subjected to sulfate attack with optical fiber excitation Raman spectroscopy

**Yanfei Yue**
**Yun Bai**
University College London
Department of Civil, Environmental and Geomatic Engineering
Gower Street, London WC1E 6BT, United Kingdom

**P. A. Muhammed Basheer**
Queen's University Belfast
School of Planning, Architecture and Civil Engineering
University Road, Belfast BT9 5AG, United Kingdom

**John J. Boland**
Trinity College Dublin
Department of Chemistry
Centre for Research on Adaptive Nanostructures and Nanodevices (CRANN)
Dublin 2, Dublin, Ireland

**Jing Jing Wang**
Trinity College Dublin
Centre for Research on Adaptive Nanostructures and Nanodevices (CRANN)
Dublin 2, Dublin, Ireland
E-mail: jjwang@tcd.ie

**Abstract.** Formation of ettringite and gypsum from sulfate attack together with carbonation and chloride ingress have been considered as the most serious deterioration mechanisms of concrete structures. Although electrical resistance sensors and fiber optic chemical sensors could be used to monitor the latter two mechanisms *on site*, currently there is no system for monitoring the deterioration mechanisms of sulfate attack. In this paper, a preliminary study was carried out to investigate the feasibility of monitoring sulfate attack with optical fiber excitation Raman spectroscopy through characterizing the ettringite and gypsum formed in deteriorated cementitious materials under an optical fiber excitation + objective collection configuration. Bench-mounted Raman spectroscopy analysis was also conducted to validate the spectrum obtained from the fiber-objective configuration. The results showed that the expected Raman bands of ettringite and gypsum in the sulfate-attacked cement paste can be clearly identified by the optical fiber excitation Raman spectrometer and are in good agreement with those identified from bench-mounted Raman spectrometer. Therefore, based on these preliminary results, it is considered that there is a good potential for developing an optical fiber-based Raman system to monitor the deterioration mechanisms of concrete subjected to sulfate attack in the future.  [DOI: 10.1117/1.OE.52.10.104107]

Subject terms: concrete durability; deterioration mechanisms; ettringite; gypsum; optical fiber excitation Raman spectroscopy; sensor; structural health monitoring; sulfate attack.

Paper 130589P received Apr. 15, 2013; revised manuscript received Sep. 8, 2013; accepted for publication Sep. 27, 2013; published online Oct. 23, 2013.

## 1 Introduction

Concrete, during its working life, is undergoing various interactions with the environment in the forms of water penetration, ion, and gas diffusion. As a result, several durability problems, such as carbonation,[1] chloride ingress,[2] and sulfate attack[3,4] could be induced. These three deterioration mechanisms are the main culprits for the degradation of concrete durability. Among these, the intrusion of $CO_2$ can cause the destruction of the high alkaline environment (pH $\approx$ 12.5) in concrete, which will ultimately cause the corrosion of steel bar. The ingress of chloride ions into structural concretes also can cause the corrosion of steel reinforcement. On the other hand, sulfate attack, an extremely complex phenomenon, is induced by a variety of erosive sources (external and internal ions) and intricate physico-chemical mechanisms. It is generally agreed that the damage caused by the sulfate attack usually arises from the formation of ettringite,[3] gypsum,[5] and thaumasite.[6] Ettringite is formed from the reactions between ingressive sulfate ions and aluminate hydrates (e.g., tricalcium aluminate hydrates and monosulfoaluminate) and unreacted aluminate or ferrite phase. The formation of ettringite is accompanied by local volume increase and subsequent pressure build-up in the surrounding matrix, leading to cracking, spalling, and even destruction of cementitious materials. In addition, ingressive sulfate ions can also react with calcium hydroxide to form gypsum. Although gypsum formation is generally accepted to be harmful (e.g., softening effect), its specific mechanism is still not well understood and the idea that gypsum formation could lead to expansion is still under debate.[5,7] Moreover, the thaumasite form of sulfate attack (TSA), a much more severe phenomenon than conventional forms of sulfate attack, usually occurs in the field, especially in buried structures.[6,8] The formation of thaumasite is a calcium silicate hydrate (C-S-H) consumptive reaction in the presence of $SO_4^{2-}$ and $CO_3^{2-}$ ions under relatively low temperature ($\leq$ 15°C) and high humidity, which can cause the total transformation of the cement matrix into white and incohesive mushy substances. As C-S-H is the main binding phase in concrete, TSA can, thus, result in losing the strength carrying capacity of concrete. Therefore, the complex nature of the above mechanisms has made the sulfate attack indeed a "confused world" and a lot of "knowledge and understanding of sulfate attack in the field remains inadequate."[9] Attempts have been made in the past to trace the ongoing deterioration mechanisms *on site*, especially the monitoring of the above-mentioned deterioration mechanisms in order to predict the serviceability and health conditions of structures. In particular, structural health monitoring, a nondestructive inspection based on the application of sensors, has been accepted as a useful tool for real-

time monitoring of concrete durability in the past two decades.[10,11]

Currently, two important sensor systems are applied for monitoring the carbonation and chloride ingress of concrete, namely, electrical resistance sensors (ERS)[12,13] and fiber optic chemical sensors (FOS).[14,15] The principle of ERS relies on the measurement of the change in the electrical resistance of concrete, which could be attributed to many reasons such as moisture variation, ingress of different substances ($Cl^-$ or $CO_2$), and ongoing hydration. Therefore, the ERS cannot differentiate each individual deterioration mechanism. On the other hand, research on FOS have been focused on development of fiber optic chloride sensors and fiber optic pH sensors, which could be used to measure the chloride ingress and pH change due to carbonation, respectively. Generally, the sensing mechanisms of these FOS depend on coating a specific chemical matrix, which has been impregnated with chloride or pH-sensitive indicator dye on the sensor/fiber tip through sol-gel techniques or the application of porous disc. The ingress of chloride or the carbonation process can change the color of the chemical dye, which can then be measured by the absorbance of light passing through the fiber using a UV-spectrophotometer. Although FOS could be applied in identifying specific deterioration mechanisms such as chloride ingress and pH change due to carbonation, their long-term stability and the need for recalibration are the two main limitations for their eventual application in the real world. However, neither sensor can be used to monitor sulfate attack. In fact, no sensor is currently available for monitoring the sulfate attack in concrete.

Raman spectroscopy, based on the measurement of the vibrational spectra of analytes, has demonstrated its effectiveness in distinguishing various sulfate-bearing products, such as ettringite,[16,17] gypsum,[18–21] and thaumasite.[22] Under Raman spectroscopy, all internal vibration modes [i.e., symmetric stretching ($\nu_1$), symmetric bending ($\nu_2$), asymmetric stretching ($\nu_3$), and asymmetric bending ($\nu_4$)] of $SO_4^{2-}$ ionic groups in gypsum and ettringite can be readily identified, while the $SO_4^{2-}$, $CO_3^{2-}$ groups and Si[22] in thaumasite also can be clearly characterized. Furthermore, Raman spectroscopy has also demonstrated its unique advantages over any other analytical techniques in differentiating these three sulfate-bearing phases due to the following unique features: (1) gypsum can be readily distinguished via its most intense peak, $\nu_1$, at 1008 $cm^{-1}$, which differs markedly from the $\nu_1$ bands of ettringite (988 $cm^{-1}$) and thaumasite (990 $cm^{-1}$). At the same time, the potential splitting of $\nu_2$ and $\nu_4$ vibrations of gypsum and its unique translational mode, i.e., $T(H_2O, Ca)$, can also be used as additional indicators to differentiate gypsum from the other sulfate-bearing products; (2) although the sulfate peaks ($\nu_1$) for ettringite and thaumasite are similar, the thaumasite can be readily differentiated from the ettringite by its distinct peaks at 658 and 1072 $cm^{-1}$, corresponding to the octahedral coordination of Si and carbonates, respectively.[22]

In recent years, with the advancement of the radiation transmission through optical fiber, the combination of Raman spectroscopy with optical fiber assemblies is now technically feasible, offering a unique opportunity for remote real-time monitoring. So far, optical fiber Raman technology has been applied in various areas, such as biomedical diagnosis,[23,24] chemistry process monitoring,[25] and even detrimental environment operations.[26] However, it has not been used to monitor concrete structures. Some feasibility studies on using optical fiber Raman spectroscopy to monitor the concrete subjected to various deterioration mechanisms have been carried out by the authors. In this paper, gypsum and ettringite, the most commonly formed deterioration products in sulfate attack, were characterized using a Raman spectrometer with fiber assembly as excitation path (hereafter, optical fiber excitation Raman spectroscopy/spectrometer). The results were also compared and verified with bench-mounted Raman analysis. Due to the complex nature and intricate environment needed to initiate its formation, the ongoing work on TSA will be reported separately. Based on the results reported in this paper, the feasibility and potential of optical fiber Raman spectroscopy as a remote characterizing and monitoring technique for concrete durability are then discussed.

## 2 Experimental Details

### 2.1 *Materials*

The Portland cement (PC) used in this study was CEM I (in accordance with BS EN 197-1:2011) supplied by Quinn Cement (Derrylin, UK) and its chemical composition is given in Table 1. Superfine white powder gypsum, supplied by Saint-Gobain Formula (Kutzhütte, Federal Republic of Germany) (300 micron sieve residue of 0.2% max), with compacted bulk density of 1200 $kg/m^3$, was employed as a reference for pure gypsum. Chemical regent CaO and $Al_2(SO_4)_3 \cdot 18H_2O$ obtained from Fisher Scientific (Loughborough, UK) were used to synthesize the pure ettringite as detailed below. Analytical grade sodium sulfate ($Na_2SO_4$) with assay (alkalimetric) >99.0% and loss on ignition (800°C) <0.5%, supplied by Merck Schuchardt OHG (Darmstadt, Germany), was used to prepare the deterioration salt solution.

### 2.2 *Samples Analyzed*

In order to identify the feasibility of optical fiber excitation Raman spectroscopy for analyzing the sulfate-attack products formed in hardened cement, two types of samples were analyzed in this study.

1. Pure sulfate-bearing samples: Prior to the characterization of the sulfate products formed in the hardened cement sample (as detailed below), one pure gypsum sample and one pure ettringite sample were first analyzed under bench-mounted Raman spectrometer so that the spectra obtained can be used to verify the results from the optical fiber system. The gypsum supplied by Saint-Gobain Formula (as mentioned in Sec. 2.1) was employed as the pure gypsum sample.

**Table 1** Chemical composition of Portland cement.

| Oxides | $SiO_2$ | $Al_2O_3$ | $Fe_2O_3$ | CaO | MgO | $K_2O$ | $Na_2O$ | $SO_3$ |
|---|---|---|---|---|---|---|---|---|
| Content/% | 23.00 | 6.15 | 2.95 | 61.30 | 1.80 | 0.68 | 0.22 | 2.50 |

The pure ettringite sample was synthesized according to the Struble's method as follows:[27] (a) 13.4 g of CaO was dissolved in 890 mL 10% w/v sucrose solution. (b) 26.55 g of $Al_2(SO_4)_3 \cdot 18H_2O$ was dissolved in 40 mL deionized water. (c) These two solutions were mixed and then put in a plastic bottle with the rest of the bottle being filled with nitrogen gas. After being tightly sealed, the bottle was put into the rotator and kept rotating for 24 h before the ettringite was isolated by suction filtration and dried under vacuum desiccators.

2. Hardened cement sample after being subjected to sulfate attack: The cement paste was manufactured at a water-to-cement ratio (W/C) of 0.35 using a Hobart planetary mixer and cast in plastic centrifugal tubes and vibrated for around 1 min to remove the air bubbles. After 24 h initial curing in the tubes, specimens were removed from the tubes and covered with water saturated hessian and then sealed in plastic sample bags. These bags were then stored in a curing room at constant temperature of $20 \pm 1$°C and relative humidity of $55 \pm 5\%$ for six days. At the end of the seventh day, selected pastes were ground into powder with a fineness of 63 $\mu$m and then immersed in 0.35 M $Na_2SO_4$ solution for 10 days before being dried in a vacuum desiccator for the Raman spectroscopy tests as detailed in Secs 2.3 and 2.4 below.

### 2.3 *Bench-Mounted Raman Spectroscopy*

A bench-mounted Renishaw micro-Raman spectrometer equipped with a charged coupled device (CCD) detector was employed. The schematic diagram of the optical path of this Raman spectrometer is shown in Fig. 1. As illustrated in Fig. 1, the Raman spectrometer operates in the classical backscattering geometry. A 632.8-nm laser (helium-neon laser) was employed as an excitation source. To overcome the heterogeneous nature of cementitious material, a 10× objective with numerical aperture (N.A.) of 0.25 was purposely employed here so that larger sampling area could be analyzed. The laser beam was focused onto the sample through the objective and the laser spot diameter after focus was ~1.6 $\mu$m. The measured power at the sampling level was ~3.3 mW. The Raman shift was calibrated before each experiment using the sharp peak of silicon at 520 $cm^{-1}$. Raman spectra were recorded with exposure time of 10 s and accumulations of 10 in order to improve the signal-to-noise ratio (SNR). In this study, the bench-mounted Raman spectroscopy analysis was used to collect some basic information in order to use them as benchmark information for verifying the results obtained from the optical fiber excitation Raman spectrometer as detailed below.

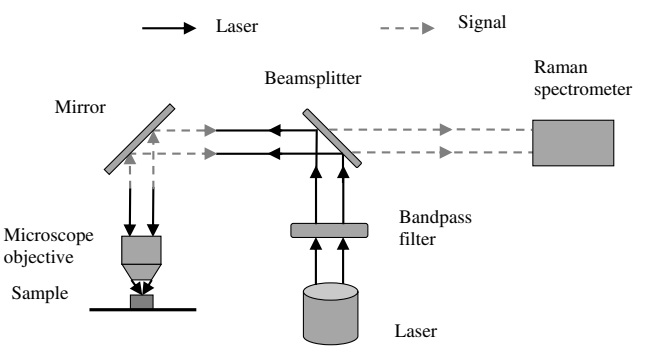


**Fig. 1** Schematic diagram of Renishaw micro-Raman spectrometer.

### 2.4 *Optical Fiber Excitation Raman Spectroscopy*

To clearly identify the coupling, transmission, excitation, and collection mechanisms in "all-fiber" Raman spectrometer, a typical 45 deg optical geometry was employed so that individual optical path (i.e., either fiber excitation path or fiber collection path) can be studied separately in order to optimize each optical path independently before an "all-fiber" Raman spectrometer could eventually be developed. This study is primarily focused on identifying the feasibility of fiber excitation approach for characterizing the sulfate attack in concrete. Therefore, a Raman spectrometer with an optical fiber as excitation path (shown in Fig. 2) was developed as detailed below.

1. Excitation subpath: The laser beam with power of 18 mW was launched into the optical fiber through an adapter, which enabled a coupling efficiency of 91% to be achieved, with a power level of 16.3 mW measured at the end of the optical fiber. A 2-m multimode fiber with core/cladding diameter of 200/240 $\mu$m and N.A. of 0.22 was employed to deliver the laser beam. After passing through the optical fiber, the divergent laser beam was collimated by a Thorlabs collimator with N.A. of 0.5. Following this, a Thorlabs 10-nm bandpass filter (centered at 632.8 nm) was installed to eliminate the scattering background generated from the optical fiber. Then the excitation laser beam was focused onto a spot of c.a. 19 $\mu$m diameter through a Thorlabs plano-convex lens with focal length of 30 mm before interrogating the sample. This tailored configuration was purposely established in order to overcome the space limitation between the stage and the objective in bench-mounted Raman spectrometer so that the signal could be collected under the 45 deg optical geometry (as mentioned below).
2. Collection subpath: The same objective (10× /0.25) and the same CCD detector as those used in the bench-mounted Raman spectrometer were again employed as the collection subpath for the optical fiber excitation Raman spectrometer. The Rayleigh scatterings launched into the objective were rejected by an edge filter in the spectrometer. Raman spectra were recorded with an exposure time of 10 s and accumulations of 10.

The excitation power of the laser after focus was measured at ~12.5 mW for the optical fiber excitation Raman spectrometer. Therefore, the excitation power densities of the optical fiber excitation Raman spectrometer and the bench-mounted Raman spectrometer were 0.04 and 1.64 mW/$\mu m^2$, respectively.

To overcome the heterogeneous nature of the cement sample, discrete multipoints were characterized and analyzed

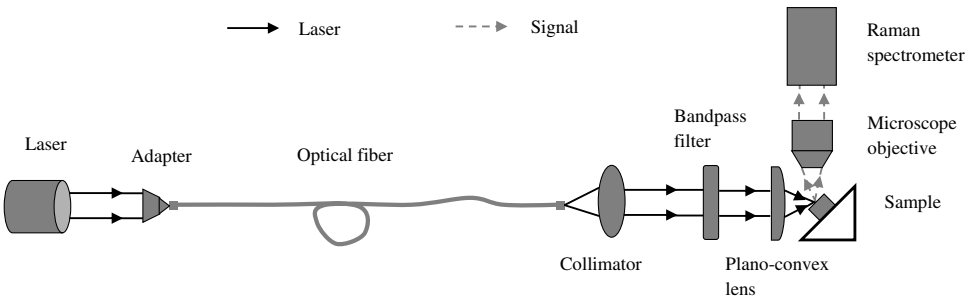


**Fig. 2** Schematic diagram of optical fiber excitation Raman spectrometer under 45 deg geometry.

under both bench-mounted Raman and optical fiber excitation Raman spectrometers. However, only one typical spectrum is presented for each optical system in order to illustrate the main features of the Raman bands. Statistical analysis in terms of the mean value, standard deviation (SD), and coefficient of variation ($\sigma$) of SNR based on the spectra from five sampling points were then calculated after background subtraction and Lorentz peak-fit using OriginPro 8.6, to compare the variations between these two optical systems.

## 3 Results and Discussion

### 3.1 *Optimization of Optical Fiber Excitation Raman Spectrometer*

Once the optical pathway described in Sec. 2.4 was preliminarily aligned, a silicon wafer was used as a reference to optimize the optical fiber excitation Raman spectrometer through the well-defined Raman peak of silicon at 520 $cm^{-1}$[28] to ensure maximum overlap between the laser excitation point and the objective focusing point is achieved. This resulted in maximum Raman peaks of silicon with highest SNR. Figure 3(a) shows the spectrum of the silicon wafer collected from this optimized optical fiber excitation Raman spectrometer, which is also compared with the spectrum of the silicon wafer collected from the bench-mounted Raman spectrometer [Fig. 3(b)] in order to verify and establish that optimum coupling and maximum overlap conditions can be achieved in the optical fiber excitation Raman spectrometer. The optical path so obtained was consequently used in the following investigations.

As can be seen from Fig. 3(a), the Raman signal of silicon has been successfully retrieved by optical fiber excitation Raman spectrometer, as indicated by a well-defined peak at 520 $cm^{-1}$ and a weak hump at approximately 920 to 1000 $cm^{-1}$. These fingerprint bands are in agreement with those from the bench-mounted Raman spectrometer, i.e., the sharp peak located at 520 $cm^{-1}$ and the weak hump near 1000 $cm^{-1}$ as shown in Fig. 3(b). After these spectra were processed with background subtraction and the Lorentz peak-fit using OriginPro 8.6, the SNR of the main peak of silicon (i.e., 520 $cm^{-1}$) were then calculated according to the method specified in ASTM E579-04.[29] The corresponding results are presented in Table 2 below.

From Table 2, the following two features can be observed:

1. Difference in signal level: The signal level of silicon fingerprint band (i.e., 520 $cm^{-1}$) under optical fiber excitation Raman spectrometer was only ~7.8% of that from bench-mounted Raman analysis. In the current study, although the power level of the optical fiber excitation Raman spectrometer was higher than that of the bench-mounted Raman spectrometer, owing to the larger excitation spot area formed under the fiber mode, the power density of the fiber mode was much lower than that of the bench-mounted Raman spectrometer (only ~2.4% of the latter as calculated in Sec. 2.4). Therefore, this reduced signal

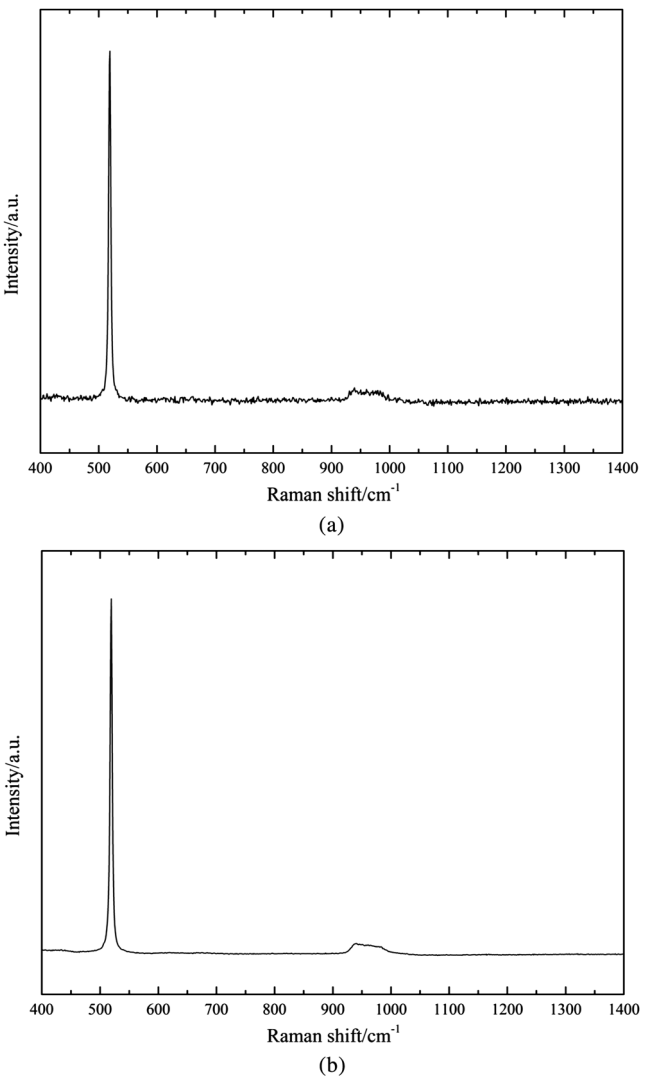


**Fig. 3** Raman spectra of silicon wafer collected from (a) optical fiber excitation Raman spectrometer and (b) bench-mounted Raman spectrometer.

**Table 2** Signal-to-noise ratio (SNR) of peak 520 $cm^{-1}$ (calculated from the spectra of Fig. 3).

| | Optical fiber excitation Raman spectroscopy | Bench-mounted Raman spectroscopy |
|---|---|---|
| Signal level | 2083.4 | 26,631.1 |
| Noise level | 9.0 | 30.9 |
| SNR | 231.5 | 861.8 |

level from the optical fiber excitation Raman spectrometer could be attributed to its lower excitation efficiency, which could be improved by increasing the power density in future studies.

2. Difference in SNR: The SNR of the optical fiber excitation Raman spectrometer was much lower than that of the bench-mounted Raman spectrometer—the SNR of the former was only ~231.5 whereas that of the latter was ~861.8 (i.e., around four times). As discussed above, the lower excitation efficiency of the optical fiber excitation mode could lead to lower signal level, which partly contributed to the reduced SNR under optical fiber excitation. On the other hand, the bench-mounted Raman spectroscopy was configured in the backscattering geometry (as shown in Fig. 1), which can maximize the overlapping between the excitation light-cone and the signal-cone, leading to a much improved collection efficiency. However, for the optical fiber excitation Raman spectrometer, the signal was collected at 45 deg configuration, which would reduce the signal collection efficiency owing to the decreased overlapping of the laser-cone and the signal-cone.

### 3.2 *Bench-Mounted Raman Spectroscopy Analysis on Gypsum and Ettringite*

To clearly identify the sulfate-attack mechanisms in cementitious materials through optical fiber excitation Raman spectroscopy, bench-mounted Raman spectroscopy was first used

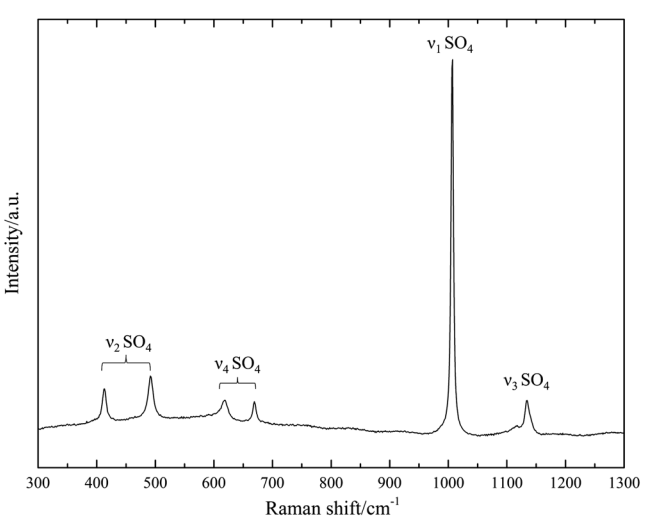


**Fig. 4** Raman spectrum of gypsum.

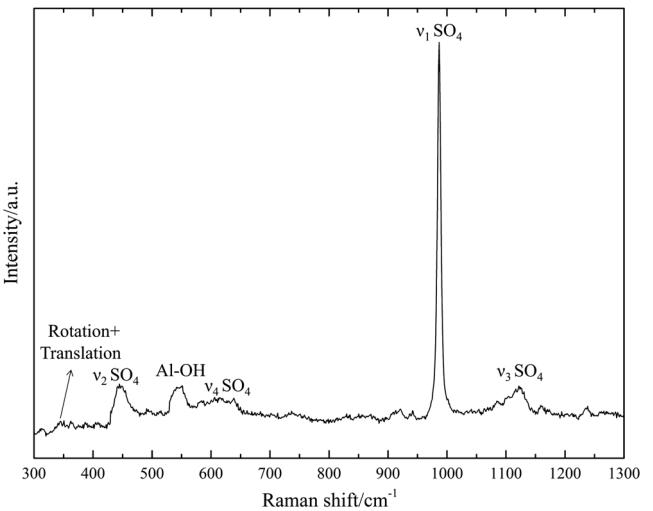


**Fig. 5** Raman spectrum of ettringite.

to characterize the pure sulfate-bearing products, i.e., gypsum and ettringite, in order to obtain benchmark spectra to verify the Raman spectrum collected from the optical fiber excitation mode in Sec. 3.3. Figures 4 and 5 show the Raman spectra of gypsum and ettringite, respectively.

As shown in Fig. 4, the Raman spectrum of gypsum was dominated by a distinct peak at 1008 $cm^{-1}$, which can be assigned to the $\nu_1$ symmetric stretching of $SO_4$ in gypsum.[18,20] The weak peak observed at 1136 $cm^{-1}$ could be attributed to the asymmetric stretching ($\nu_3$) of $SO_4$ in gypsum.[20] Furthermore, two doublets assigned to the $SO_4$ symmetric bending ($\nu_2$) and asymmetric bending ($\nu_4$) modes of gypsum, respectively,[20,21] were identified at 414/493 and 618/670 $cm^{-1}$, which are in good agreement with previously published data.[20,21] Therefore, all the four internal vibration modes of $SO_4$ of gypsum have been clearly identified by bench-mounted Raman spectroscopy with $\nu_1$ symmetric stretching mode being the most intense vibration band, which corroborates well with the literature.[30]

Characterization of ettringite with Raman spectroscopy is well established and different types of ettringite have been successfully characterized and reported in the literature. These include the ettringite formed from the hydration of tricalcium aluminate ($C_3A$) in the presence of gypsum,[16] naturally occurring crystal of ettringite,[17] as well as those synthesized under controlled laboratory conditions.[30] Generally, it has been concluded that the four internal $SO_4$ vibration modes and the Al-OH vibration mode in ettringite as well as the external rotation and translation of ettringite molecules can be clearly identified.[16,17] As shown in Fig. 5, in the current study, all the internal $SO_4$ vibration modes have been successfully identified by the bench-mounted Raman spectroscopy, as indicated by a distinct peak located at 988 $cm^{-1}$ ($\nu_1$) and three bands at 448 $cm^{-1}$ ($\nu_2$), 612 $cm^{-1}$ ($\nu_4$), and 1119 $cm^{-1}$ ($\nu_3$), respectively. At the same time, the external rotation and translation of ettringite molecules and Al-OH vibration in ettringite have also been clearly identified by the two weak humps located at 347 and 547 $cm^{-1}$, respectively.[16,17]

Table 3 summarizes and compares the Raman bands and assignments of gypsum and ettringite under bench-mounted Raman spectroscopy. As it can be seen, in addition to the Al-OH vibration, which can clearly distinguish ettringite from

**Table 3** Raman bands and assignments of pure gypsum and ettringite under bench-mounted Raman spectroscopy.

| Excitation/nm | Raman shift/cm$^{-1}$ | | Assignment |
|---|---|---|---|
| | Gypsum | Ettringite | |
| 632.8 nm | 1008 | 988 | $\nu_1$ symmetric stretching of ($SO_4$) |
| | 414, 493 | 448 | $\nu_2$ symmetric bending of ($SO_4$) |
| | 1136 | 1119 | $\nu_3$ asymmetric stretching of ($SO_4$) |
| | 618, 670 | 612 | $\nu_4$ asymmetric bending of ($SO_4$) |
| | | 347 | External rotation + translation |
| | | 547 | Al-OH stretching |

gypsum, the Raman shifts of the four internal $SO_4$ vibration modes also can be used as additional fingerprints to differentiate ettringite from gypsum as follows: (1) for the $SO_4$ symmetric stretching ($\nu_1$) and asymmetric stretching ($\nu_3$), there were wave number shifts between gypsum and ettringite, i.e., by 20 and 17 cm$^{-1}$ for $\nu_1$ and $\nu_3$, respectively; (2) for the $SO_4$ symmetric bending ($\nu_2$) and asymmetric bending ($\nu_4$) modes, two doublets were identified for gypsum at 414/493 and 618/670 cm$^{-1}$, while only two single peaks were identified at 448 and 612 cm$^{-1}$ for ettringite. These results would suggest that gypsum and ettringite can be readily differentiated by Raman spectroscopy, which is in good agreement with the previously published results in the literature.[16,17,20]

### 3.3 *Bench-Mounted Raman Spectroscopy/Optical Fiber Excitation Raman Spectroscopy Analysis on Sulfate-Attacked Cement Sample*

In Sec. 3.2, the Raman bands of pure gypsum and ettringite have been clearly identified, which are to be used as benchmark information in the following studies for characterizing the gypsum and the ettringite formed in the sulfate-attacked cement sample. While the Raman bands can be readily identified in pure and white-colored gypsum and ettringite samples, it could potentially be difficult to characterize these in the sulfate-attacked cement pastes due to the gray color and heterogeneous nature of PC. In addition, the existence of certain impurities in the unhydrated cement minerals could induce strong fluorescence background, which can impose disturbance to or even totally swamp the weak Raman peaks.[31] In the current study, further complexities could also occur from the transmission of laser light through optical fiber as troublesome background could be induced from the fiber core. In addition, the collimation of the output divergent laser at the end of the optical fiber is also an issue. Therefore, to clearly identify the feasibility and efficiency of optical fiber system for identifying sulfate-attack products in hardened cements, bench-mounted Raman spectroscopy analysis was first carried out, which was then followed by optical fiber excitation Raman spectroscopy analysis using the optical fiber pathway developed in Sec. 3.1.

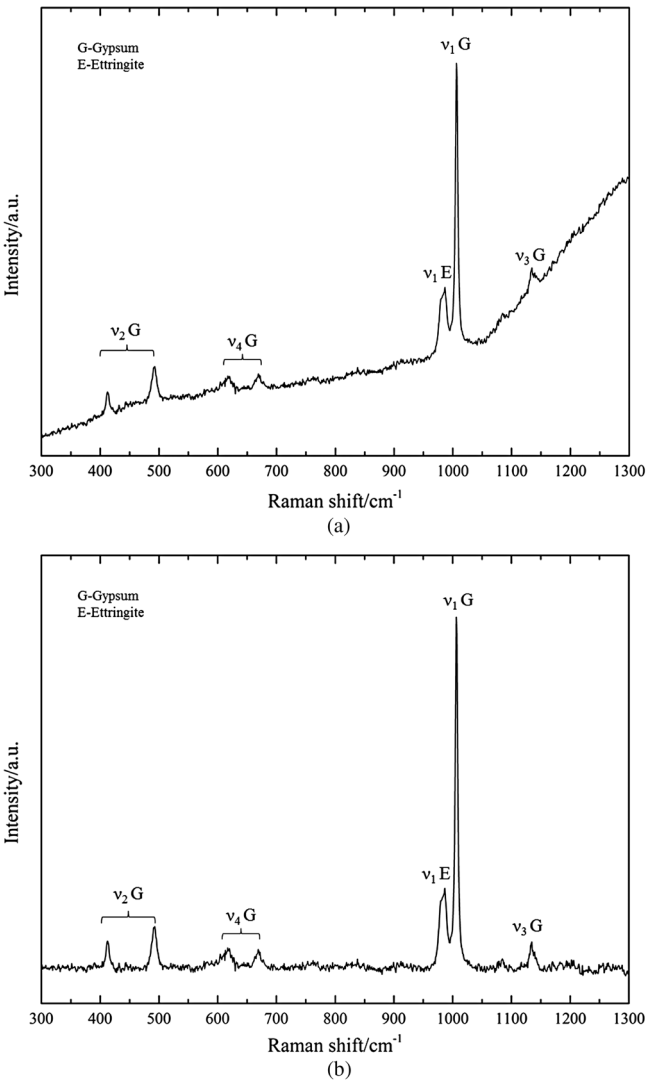


**Fig. 6** Raman spectra of sulfate-attacked sample of (a) original spectrum and (b) spectrum after subtracting the background.

Figures 6(a) and 7(a) present the Raman spectra of sulfate-attacked cement pastes under bench-mounted Raman and optical fiber excitation Raman analysis, respectively. As expected, compared with Figs. 4 and 5, sloping backgrounds can be observed in the original spectra collected from the cement sample. In Fig. 6(a), a sloping background emerged from 300 cm$^{-1}$ onward, imposing a strong disturbance to the Raman spectrum—especially to the band located at 1136 cm$^{-1}$ ($\nu_3$ $SO_4$), which was nearly swamped by this background. On the other hand, an even stronger background could be observed from the optical fiber spectrum in Fig. 7(a), indicating that some additional issues have been induced by the optical fiber system. Baseline correction using OriginPro 8.6 was, therefore, applied in an attempt to reduce the background effect,[32] and the resultant spectra are shown in Figs. 6(b) and 7(b), respectively. It can be seen that after subtracting the background, all the Raman bands became more evident. Therefore, spectra with subtracted background were used for further analysis and discussion below.

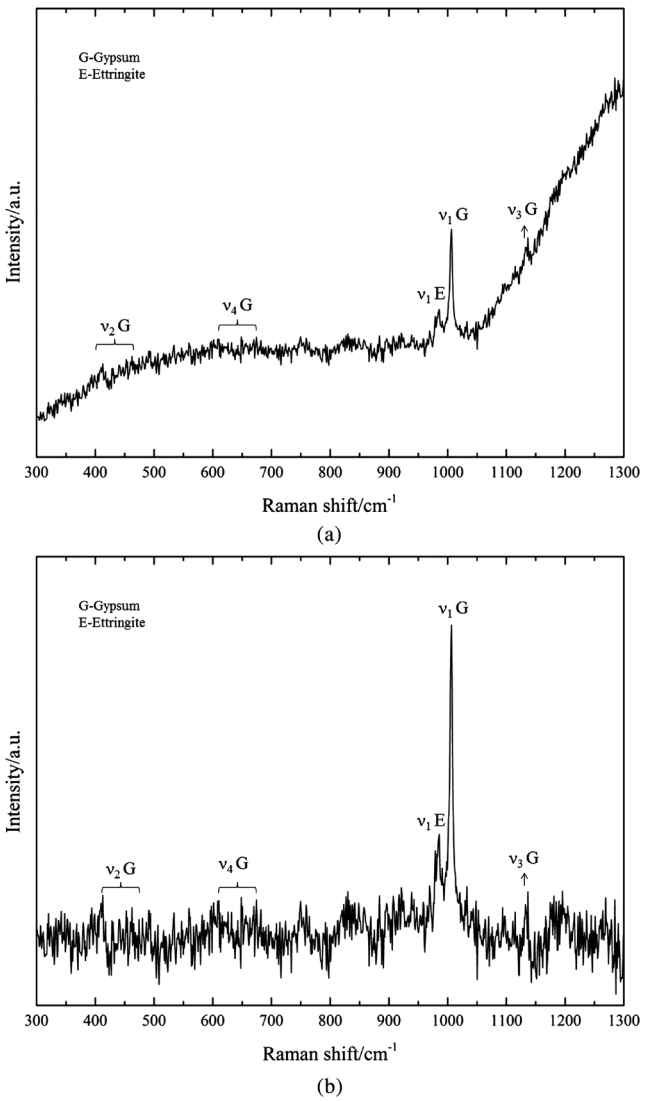


**Fig. 7** Optical fiber excitation Raman spectra of sulfate-attacked sample of (a) original spectrum and (b) spectrum after subtracting the background.

From Fig. 6(b), it can be seen that the gypsum formed in the sulfate-attacked cement paste has been successfully identified as indicated by its four $SO_4$ internal vibration bands retrieved at 1007 cm$^{-1}$ ($\nu_1$ symmetric stretching), 1136 cm$^{-1}$ ($\nu_3$ asymmetric stretching), 414/493 cm$^{-1}$ ($\nu_2$ symmetric bending), and 617/670 cm$^{-1}$ ($\nu_4$ asymmetric bending), respectively.[20,21] At the same time, ettringite has also been identified as indicated by its $SO_4$ $\nu_1$ symmetric stretching band located at 986 cm$^{-1}$.[16] The main Raman bands and assignments of the spectrum in Fig. 6(b) are further summarized in Table 4. By comparing Tables 3 and 4, it can be noticed that similar Raman peaks have been identified for the sulfate-bearing crystals (i.e., ettringite and gypsum) in both the sulfate-attacked cement paste and the pure sulfate-bearing samples (as reported in Sec. 3.2). The similarity in these peaks suggests that similar gypsum and ettringite products have been formed in the sulfate-attacked cement paste and these can be readily identified by Raman spectroscopy. The strong gypsum peak also indicated that considerable sulfate-attack mechanism has been formed in $Na_2SO_4$ solution.[33] On the other hand, the identified ettringite could be attributed to the secondary ettringite (i.e., ettringite formed under sulfate-attack mechanisms) or the primary ettringite (i.e., ettringite generated shortly after cement hydration) in the current study.

**Table 4** Raman bands and assignments of sulfate-attacked cement sample under optical fiber excitation spectroscopy and bench-mounted Raman spectroscopy.

| | Raman shift/cm$^{-1}$ | Assignments |
|---|---|---|
| Optical fiber excitation Raman spectroscopy | 1007 | $\nu_1$ ($SO_4$) (gypsum) |
| | 410 | $\nu_2$ ($SO_4$) (gypsum) |
| | 493 | $\nu_2$ ($SO_4$) (gypsum) |
| | 1134 | $\nu_3$ ($SO_4$) (gypsum) |
| | 608 | $\nu_4$ ($SO_4$) (gypsum) |
| | 667 | $\nu_4$ ($SO_4$) (gypsum) |
| | 986 | $\nu_1$ ($SO_4$) (ettringite) |
| Bench-mounted Raman spectroscopy | 1007 | $\nu_1$ ($SO_4$) (gypsum) |
| | 414 | $\nu_2$ ($SO_4$) (gypsum) |
| | 493 | $\nu_2$ ($SO_4$) (gypsum) |
| | 1136 | $\nu_3$ ($SO_4$) (gypsum) |
| | 617 | $\nu_4$ ($SO_4$) (gypsum) |
| | 670 | $\nu_4$ ($SO_4$) (gypsum) |
| | 986 | $\nu_1$ ($SO_4$) (ettringite) |

Figure 7(b) demonstrates the Raman spectrum of sulfate-attacked sample retrieved from the optical fiber excitation Raman system after subtracting the background. As shown in Fig. 7(b), after background subtraction, various Raman bands, which were previously obscured by the strong fluorescence background in the original spectrum in Fig. 7(a), can now be clearly identified—especially the various weak peaks that lay between 400 and 500 cm$^{-1}$ and 600 and 700 cm$^{-1}$ and the peak at 1134 cm$^{-1}$. In particular, compared with the spectrum in Fig. 7(a), the Raman shifts of gypsum at 1007 cm$^{-1}$ ($\nu_1$ symmetric stretching) and 1134 cm$^{-1}$ ($\nu_3$ asymmetric stretching) and the two doublets at 410/493 cm$^{-1}$ ($\nu_2$ symmetric bending), and 608/667 cm$^{-1}$ ($\nu_4$ asymmetric bending) became more evident.[20,21] In addition, the Raman bands of $SO_4$ vibration in ettringite can also be clearly identified as a sharp peak at 986 cm$^{-1}$ ($\nu_1$).[16,17] It has been generally agreed that fluorescence is one of the most troublesome issues hindering the application of Raman spectroscopy in cementitious materials.[31,34] As indicated before, the introduction of optical fiber in the current study can further complicate matters. Therefore, this much improved visibility of Raman peaks in Fig. 7(b) after background subtraction would suggest again that background subtraction is a useful technique for processing the Raman spectra of cementitious materials,

**Table 5** Statistic of peaks from sulfate-attacked sample under bench-mounted Raman analysis.

| Sampling point | $\nu_1$(E) | Signal level | Mean of signal | Noise level | Mean of noise | SNR | Mean of SNR | Standard deviation of SNR | Coefficient of variation of SNR |
|---|---|---|---|---|---|---|---|---|---|
| Point 1 | 986 | 2335.4 | 2628.0 | 72.5 | 97.0 | 32.2 | 27.4 | 4.1 | 15.0% |
| Point 2 | 986 | 1987.4 | | 87.1 | | 22.8 | | | |
| Point 3 | 985 | 2890.2 | | 93.1 | | 31.0 | | | |
| Point 4 | 987 | 2687.4 | | 109.0 | | 24.7 | | | |
| Point 5 | 985 | 3239.6 | | 123.1 | | 26.3 | | | |

**Table 6** Statistic of peaks from sulfate-attacked sample under optical fiber excitation Raman analysis.

| Sampling point | $\nu_1$(E) | Signal level | Mean of signal | Noise level | Mean of noise | SNR | Mean of SNR | Standard deviation of SNR | Coefficient of variation of SNR |
|---|---|---|---|---|---|---|---|---|---|
| Point 1 | 986 | 234.3 | 241.2 | 50.4 | 46.2 | 4.6 | 5.2 | 0.6 | 11.5% |
| Point 2 | 986 | 209.0 | | 41.9 | | 5.0 | | | |
| Point 3 | 986 | 286.4 | | 47.1 | | 6.1 | | | |
| Point 4 | 987 | 236.9 | | 44.2 | | 5.4 | | | |
| Point 5 | 986 | 239.6 | | 47.5 | | 5.0 | | | |

especially for those obtained from the optical fiber excitation Raman spectrometer.

Table 4 compares the Raman bands and assignments of the spectra obtained from the sulfate-attacked cement sample under both optical fiber excitation spectroscopy and bench-mounted Raman spectroscopy. It can be seen that, although the fingerprint peaks collected from both bench-mounted and optical fiber Raman spectroscopy were very similar, a tiny wave number shift can be observed from optical fiber results compared with the bench-mounted Raman spectroscopy. For example, the $SO_4$ $\nu_3$ mode of gypsum was 1136 $cm^{-1}$ under bench-mounted Raman, but 1134 $cm^{-1}$ under optical fiber excitation Raman system. This could be attributed to the heterogeneous nature of the cementitious materials, making it almost impossible to test two identical areas.

As mentioned before, to overcome the heterogeneous nature of the cement sample, discrete multipoints were characterized and analyzed. To illustrate this feature, one of the vibration modes, $\nu_1$ $SO_4$ of ettringite, was selected for statistical analysis. The spectra of five sampling points were selected and the statistic calculation in terms of mean value, standard deviation (SD), and the coefficient of variation ($\sigma$) of SNR was then carried out. Tables 5 and 6 present the statistical analysis results of bench-mounted Raman spectroscopy and optical fiber Raman system, respectively, which indicate the following:

1. Both the mean values of the signal level and the noise level were lower in optical fiber excitation Raman spectroscopy. The SNR values showed a similar tendency—only 5.2 under optical fiber Raman spectroscopy, but as high as 27.4 under bench-mounted system. These results could be attributed to the lower excitation power density and the lower signal collection efficiency in optical fiber excitation Raman system as discussed in Sec. 3.1.
2. The SD of SNR under optical fiber excitation Raman spectroscopy was much lower than that under bench-mounted Raman system—the former was only 0.6 while the latter was 4.1. At the same time, the coefficient of variation ($\sigma$) of fiber mode was much lower as well. The lower SD and $\sigma$ suggests the lower variation and higher reliability of data sampling under optical fiber excitation Raman spectroscopy. One possible explanation for these results is the relatively larger sampling area (283.4 $\mu m^2$) of optical fiber excitation Raman system as compared with that of bench-mounted Raman system (2.0 $\mu m^2$), resulting in more Raman information being retrieved from the heterogeneous sample.[35]

Therefore, our results clearly showed the advantage of the optical fiber excitation Raman spectroscopy as developed in this paper over the bench-mounted Raman spectroscopy for characterizing heterogeneous matrix.

## 4 Conclusions

Inspired by the successful application of optical fiber Raman spectroscopy in biomedical diagnosis and chemistry monitoring, this research is primarily focused on identifying the feasibility of this technique in remote characterizing cementitious materials, which will eventually lead to the development of a novel concrete durability monitoring system. One of the most important concrete deterioration

mechanisms, sulfate attack, was investigated in the current study and the two most important sulfate-bearing products, i.e., gypsum and ettringite, formed in sulfate-attacked cementitious materials have been successfully differentiated by a pilot optical fiber excitation system (45 deg geometry) configured with an optical fiber as the excitation subpath. Under the optical fiber excitation Raman spectroscopy, the four $SO_4$ vibration bands of the gypsum formed in sulfate-attacked cement paste have been successfully identified at 1007 $cm^{-1}$ ($\nu_1$), 1134 $cm^{-1}$ ($\nu_3$), 410/493 $cm^{-1}$ ($\nu_2$), and 608/667 $cm^{-1}$ ($\nu_4$), which are in good agreement with the bench-mounted analysis results; in the case of ettringite, the $\nu_1$ band was identified at 986 $cm^{-1}$ under the fiber excitation mode. Therefore, this preliminary study indicated that it is technically feasible to characterize the sulfate-induced deterioration mechanisms in cementitious materials using optical fiber excitation Raman spectroscopy. Although the fingerprint bands collected from the optical fiber excitation Raman system showed weaker signal level and lower SNR, their standard deviation and coefficient of variation were lower, showing good potential for characterizing heterogeneous matrix like concrete.

## Acknowledgments

The authors would like to acknowledge the support received from the EPSRC UK-China Science Bridge project. The access to the photonics laboratory at CRANN for part of this project was funded by the Higher Education Authority in Ireland via PRTLI4. Miss Yanfei Yue is currently sponsored by China Scholarship Council and Faculty of Engineering Postgraduate Research Scholarship for her PhD study in University College London, United Kingdom. The CEM I Portland cement used in this research was supplied by Quinn Cement.

## References

1. V. G. Papadakis, C. G. Vayenas, and M. N. Fardis, "Experimental investigation and mathematical modeling of the concrete carbonation problem," *Chem. Eng. Sci.* **46**(5/6), 1333–1338 (1991).
2. K. Thangavel and N. Rengaswamy, "Relationship between chloride/hydroxide ratio and corrosion rate of steel in concrete," *Cement Concr. Comp.* **20**(4), 283–292 (1998).
3. E. F. Irassar, V. L. Bonavetti, and M. González, "Microstructural study of sulfate attack on ordinary and limestone Portland cements at ambient temperature," *Cement Concr. Res.* **33**(1), 31–41 (2003).
4. N. Crammond, "The occurrence of thaumasite in modern construction—a review," *Cement Concr. Comp.* **24**(3–4), 393–402 (2002).
5. B. Tian and M. D. Cohen, "Does gypsum formation during sulfate attack on concrete lead to expansion?," *Cement Concr. Res.* **30**(1), 117–123 (2000).
6. N. J. Crammond, "The thaumasite form of sulfate attack in the UK," *Cement Concr. Comp.* **25**(8), 809–818 (2003).
7. D. Bonen, "A microstructural study of the effect produced by magnesium sulfate on plain and silica fume-bearing Portland cement mortars," *Cement Concr. Res.* **23**(3), 541–553 (1993).
8. D. W. Hobbs and M. G. Taylor, "Nature of the thaumasite sulfate attack mechanism in field concrete," *Cement Concr. Res.* **30**(4), 529–533 (2000).
9. A. Neville, "The confused world of sulfate attack on concrete," *Cement Concr. Res.* **34**(8), 1275–1296 (2004).
10. H. N. Li, D. S. Li, and G. B. Song, "Recent applications of fiber optic sensors to health monitoring in civil engineering," *Eng. Struct.* **26**(11), 1647–1657 (2004).
11. J. Ko and Y. Ni, "Technology developments in structural health monitoring of large-scale bridges," *Eng. Struct.* **27**(12), 1715–1725 (2005).
12. W. J. McCarter, M. Emerson, and H. Ezirim, "Properties of concrete in the cover zone: developments in monitoring techniques," *Mag. Concr. Res.* **47**(172), 243–251 (1995).
13. W. J. McCarter et al., "Near-surface sensors for condition monitoring of cover-zone concrete," *Constr. Build. Mater.* **15**(2), 115–124 (2001).
14. P. A. M. Basheer et al., "Fibre optic chemical sensor systems for monitoring pH changes in concrete," *Proc. SPIE* **5586**, 144–153 (2004).
15. W. Xie et al., "Fibre optic chemical sensor systems for internal concrete condition monitoring," *Proc. SPIE* **5502**, 334–337 (2004).
16. L. Black et al., "*In situ* Raman analysis of hydrating $C_3A$ and $C_4AF$ pastes in presence and absence of sulphate," *Adv. Appl. Ceram.* **105**(4), 209–216 (2006).
17. S. Deb et al., "Raman scattering and X-ray diffraction study of the thermal decomposition of an ettringite-group crystal," *Phys. Chem. Miner.* **30**(1), 31–38 (2003).
18. E. Knittle, W. Phillips, and Q. Williams, "An infrared and Raman spectroscopic study of gypsum at high pressures," *Phys. Chem. Miner.* **28**(9), 630–640 (2001).
19. P. S. R. Prasad, A. Pradhan, and T. N. Gowd, "*In situ* micro-Raman investigation of dehydration mechanism in natural gypsum," *Curr. Sci.* **80**(9), 1203–1207 (2001).
20. S. N. White, "Laser Raman spectroscopy as a technique for identification of seafloor hydrothermal and cold seep minerals," *Chem. Geol.* **259**(3), 240–252 (2009).
21. N. Buzgar, A. Buzatu, and I. V. Sanislav, "The Raman study on certain sulfates," *An. Stiint. U. Al. I-Mat.* **55**(1), 5–23 (2009).
22. A. R. Brough and A. Atkinson, "Micro-Raman spectroscopy of thaumasite," *Cement Concr. Res.* **31**(3), 421–424 (2001).
23. J. T. Motz et al., "Optical fiber probe for biomedical Raman spectroscopy," *Appl. Opt.* **43**(3), 542–554 (2004).
24. M. G. Shim et al., "Study of fiber-optic probes for *in vivo* medical Raman spectroscopy," *Appl. Spectrosc.* **53**(6), 619–627 (1999).
25. J. F. Aust, K. S. Booksh, and M. L. Myrick, "Novel *in situ* probe for monitoring polymer curing," *Appl. Spectrosc.* **50**(3), 382–387 (1996).
26. M. Myrick et al., "*In situ* fiber-optic Raman spectroscopy of organic chemistry in a supercritical water reactor," *J. Raman Spectrosc.* **25**(1), 59–65 (1994).
27. E. Ciliberto, S. Ioppolo, and F. Manuella, "Ettringite and thaumasite: a chemical route for their removal from cementious artefacts," *J. Cult. Herit.* **9**(1), 30–37 (2008).
28. J. H. Parker, Jr., D. W. Feldman, and M. Ashkin, "Raman scattering by silicon and germanium," *Phys. Rev.* **155**(3), 712 (1967).
29. ASTM Standard E 579-04, Standard Test Method for Limit of Detection of Fluorescence of Quinine Sulfate in Solution.
30. G. Renaudin et al., "A Raman study of the sulfated cement hydrates: ettringite and monosulfoaluminate," *J. Adv. Concr. Technol.* **5**(3), 299–312 (2007).
31. C. D. Dyer, P. J. Hendra, and W. Forsling, "The Raman spectroscopy of cement minerals under 1064 nm excitation," *Spectrochim Acta A-M* **49**(5–6), 715–722 (1993).
32. J. Zhao et al., "Automated autofluorescence background subtraction algorithm for biomedical Raman spectroscopy," *Appl. Spectrosc.* **61**(11), 1225–1232 (2007).
33. M. Santhanam, M. D. Cohen, and J. Olek, "Effects of gypsum formation on the performance of cement mortars during external sulfate attack," *Cement Concr. Res.* **33**(3), 325–332 (2003).
34. S. P. Newman et al., "Anomalous fluorescence in near-infrared Raman spectroscopy of cementitious materials," *Cement Concr. Res.* **35**(8), 1620–1628 (2005).
35. M. Kim et al., "New reliable Raman collection system using the wide area illumination (WAI) scheme combined with the synchronous intensity correction standard for the analysis of pharmaceutical tablets," *Anal. Chim Acta.* **579**(2), 209–216 (2006).

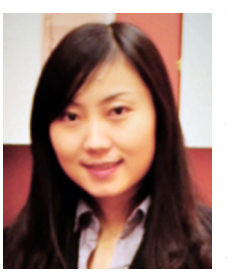

**Yanfei Yue** is a PhD student in the Department of Civil, Environmental and Geomatic Engineering at University College London (UCL), UK. She is also a member of the Advanced & Innovative Materials (AIM) Group led by Dr. Yun Bai (also her principal supervisor) in UCL. She received both of her BSc and MSc degrees in Building Materials from Chongqing University, China. Her current PhD research is on the application of optical fiber Raman spectroscopy in Civil Engineering, especially on monitoring the durability of concrete structures.

**Yun Bai** is a senior lecturer in materials and head of the advanced and innovative materials (AIM) research group in the Department of Civil, Environmental and Geomatic Engineering (CEGE) at University College London (UCL), UK. He received his BSc degree in building materials from Chongqing University, China, a MSc in computing and information systems (Distinction) from University of Ulster, UK and a PhD in construction materials from Queen's University Belfast, UK. Prior to his MSc and

PhD studies in the UK in 2000, he had been working as an associate civil engineer/civil engineer and project manager in China for over 7 years. After his PhD study in 2004, he worked as a postdoctoral research associate in The University of Sheffield and then joined Queen's University Belfast as a lecturer in civil engineering in 2007 before taking his present post in UCL in early 2012. His current research profile can be summarized as 'industry driven and interdisciplinary,' which covers a wide range of material science and engineering properties of materials including novel low-carbon cement and concrete, concrete durability, nuclear waste immobilization, structural health monitoring and nondestructive testing of structural concrete. He is a member of The Institute of Concrete Technology and a member of the Cementitious Materials Group Committee, The Institute of Materials, Minerals and Mining.

**P. A. Muhammed Basheer** is the chair of Structural Materials and the director of the Centre for Built Environment Research at Queen's University Belfast, Northern Ireland, United Kingdom. He is also a visiting professor at Zhejiang University and Chongqing University in China. He received his bachelors degree in civil engineering and masters degree in structural engineering, both from India and PhD in structural materials from Queen's University Belfast. He has been an educationalist and researcher in the field of civil (structural) engineering for more than 30 years. His research interests are primarily on the Science, Technology and Performance of Concrete and Concrete Structures, with special emphasis on nondestructive evaluation, structural health monitoring and performance testing of concrete structures. He is an elected fellow of the Irish Academy of Engineering, Institution of Civil Engineers and American Concrete Institute. He is also a member of numerous technical committees of both the American Concrete Institute and RILEM. He is an editor of the International Journal of Construction and Building Materials and an associate editor of the International Journal of Civil Structural Health Monitoring. He has authored more than 300 refereed technical publications and received the American Concrete Institute's ACI/James Instruments Award for best NonDestructive Testing Limited in 1990 for developing the Autoclam Permeability System and in 1999 for developing the Permit Ion Migration test.

**John J. Boland** received a BSc degree in chemistry from University College Dublin and a PhD in chemical physics from the California Institute of Technology. From 1984 to 1994 he was a member of the research staff at the IBM T.J. Watson Research Center (New York). In 1994, he joined the chemistry faculty at the University of North Carolina at Chapel Hill where he was appointed the J.J. Hermans Chair Professor of Chemistry and Applied and Materials Science. In 2002, he moved to the School of Chemistry at Trinity College Dublin as a Science Foundation Ireland Principal Investigator. In 2005, he was appointed as a director of the Centre for Research on Adaptive Nanostructures and Nanodevices (CRANN), which is Ireland's flagship nano and materials science institute. He is an internationally recognised expert in the chemistry of semiconductors surfaces and the use of scanning probe microscopy to elucidate materials and device properties. He was elected a fellow of Trinity College in 2008, a fellow of the American Vacuum Society (AVS) in 2009 and a fellow of the American Association for the Advancement of Science (AAAS) in 2010. He was the recipient of ACSIN Nanoscience Prize in 2011, St Petersburg, Russia and an ERC Advanced Grant.

**Jing Jing Wang** is a senior researcher in CRANN at Trinity College Dublin, Ireland. Prior to that, he carried out his postdoctoral researches in the University of Sheffield. He received his PhD degree in physics from the University of Leeds in 2005. He earned his MSc degree in physics from Peking University in 1998 and received his BEng degree in optical engineering from Tsinghua University in 1990. He has authored more than 80 refereed publications and his current research interests include Raman spectroscopy, fluorescence spectroscopy, near-field optics and nano-photonics.